Ultimate Strength and Failure Mechanism of Resistance Spot Weld Subjected to Tensile, Shear, or Combined Tensile/Shear Loads

Yuh J. Chao
Mem. ASME
Department of Mechanical Engineering,
University of South Carolina,
Columbia, SC 29208
e-mail: chao@sc.edu

Strength tests were performed to reveal the failure mechanisms of spot weld in lap-shear and cross tension test samples. It is shown the while the lap-shear (cross tension) sample is subjected to shear (normal) load at the structural level the failure mechanism at the spot weld is tensile (shear) mode at the materials level. Based on the observed failure mechanism, stress distribution is assumed and related to the far field load for the lap-shear and cross tension test samples. It appears that the failure load of the cross tension sample is 74 percent of the lap-shear sample based on the classical von Mises failure theory. The theoretical model is further extended to the mixed normal/shear loading condition. Data from strength tests as well as finite element numerical method are used to validate the model. Finally, the utility of the model in accessing the failure strength of spot welds is discussed. [DOI: 10.1115/1.1555648]

1 Introduction

Spot weld made by resistance welding has been widely used in joining sheet metal for auto body since 1950's and is the primary method of joining in ground vehicle industry. A modern vehicle typically contains 2000 to 5000 spot welds. The strength of the spot weld under quasi-static, impact, and fatigue loading conditions is therefore extremely important to the durability and safety design of automobiles. In this paper, we focus our attention on the failure behavior of spot weld under quasi-static overload condition.

Although the spot weld has been used extensively, a simple failure criterion that is able to predict the failure strength of a spot weld subjected to various loading conditions does not exist. Conventional practice in industry is to perform extensive tests to obtain sufficient data sets for design purpose [1,2]. The drawback of this approach is that there are simply too many variables to consider, e.g., welding parameters, sheet thickness, weld nugget size for a given material. Consequently, it is costly to develop a meaningful and useful database. A verified, mechanics based failure theory would be very useful to the designers and significantly reduce the number of test required and thus the cost involved.

Due to its complex geometry, analytical solution for stresses in a spot weld is difficult to obtain. Radaj [3], Radaj and Zhang [4], and Zhang [5–8] have adopted a fracture mechanics approach and provided very detailed stress distribution around a weld nugget. The derived linear elastic stress intensity factor solutions are mathematical in nature and its practical application to the failure of spot weld under monotonic loading has not been fully realized.

Wung [9] and Wung et al. [10] have recently reported the failure strength of spot weld under in-plane torsion and advocated the force based failure criterion which is used in commercial finite element code such as LS-DYNA3D.

Zuniga and Sheppard [11] performed failure test of spot weld on high strength steel and studied detailed failure mechanisms of lap-shear and coach peel samples. One of the main findings from their work is that the failure mechanism for lap-shear sample is localized necking (shear localization) in the base metal and near the boundary between HAZ and base metal. Because of this finding they then attempted using the plastic strain in the thickness direction near the weld nugget as the failure criterion to interpret the strength of spot weld.

Barkey et al. [12] and Lee et al. [13] designed a test sample and a fixture such that a spot weld test sample can be loaded under pure shear, mixed shear/normal, or pure normal load by changing the loading position of the fixture. Ultimate strength data of spot welds using the fixture were reported and curve fitted to a force based failure criterion for design consideration. Similarly, Lin et al. [14] reported another mixed mode test fixture and some test results.

At the University of South Carolina, weldability, failure mechanism and strength of spot weld under static, fatigue and impact loading conditions are being investigated. Since interfacial mode of failure in spot weld is generally not acceptable for automobile applications due to its low load carrying and energy absorption capability we first studied the mechanics aspect of failure mode of spot weld, i.e., under what conditions a spot weld would fail in the nonacceptable interfacial mode (or the acceptable nugget pullout mode) [15]. Having the interfacial mode of failure excluded, current paper as the second paper in the series addresses the ultimate strength and failure mechanisms of spot weld subjected to tensile, shear or combination of the two, under the assumption that the weld fails in the pullout mode. The objective of this study is to develop an engineering failure criterion for spot weld in thin sheet metals under nugget pullout mode. Failure of spot weld under impact loading as well as fatigue loading will be the subject of future reports from our investigation.

To develop the failure criterion of spot welds, we first performed the strength test using cross tension and lap-shear (or tensile-shear) samples made of a high strength steel. The cross tension (lap-shear) sample geometry is chosen as a representative case for predominantly opening (shear) load or a normal (shear) force to the weld. Observation during the test reveals the fracture initiation site and pattern. Fractographs from the fractured surface are examined and the fracture mechanisms are then identified. Based on the fracture mechanism a stress distribution is developed and related to the failure load or ultimate strength of the spot weld for the two sample geometries. A mechanics based failure criterion for the spot weld is then established using classical von Mises or Tresca criterion. Having the failure criterion for each of the two

Contributed by the Materials Division for publication in the JOURNAL OF ENGINEERING MATERIALS AND TECHNOLOGY. Manuscript received by the Materials Division February 5, 2002; revision received August 12, 2002. Associate Editor: G. Newaz.

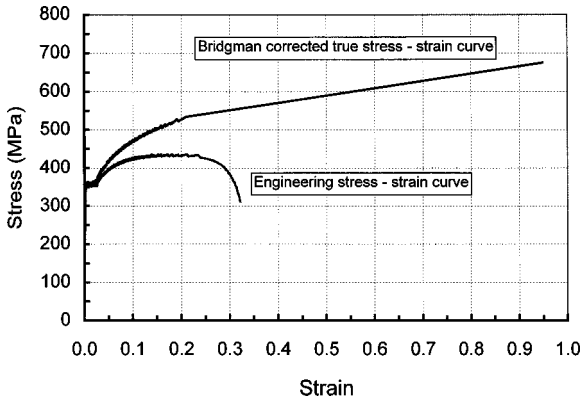

Fig. 1 Engineering and true stress-strain curves for the HSLA steel tested

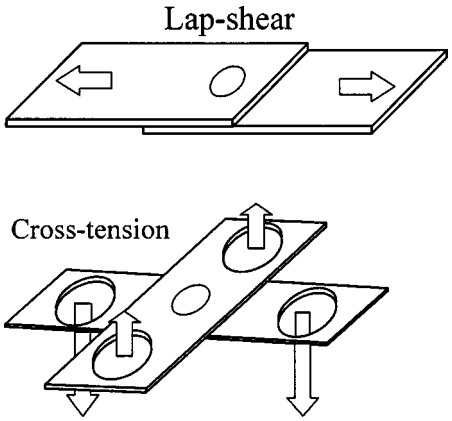

Fig. 2 Cross tension and lap-shear test sample geometries

sample geometries established, i.e., tensile and shear, we finally extend the failure criterion to combined tensile/shear loading mode. Comparison with our test data as well as those from open literature indicates that the prediction based on the developed theory is very credible. In the section of discussion, potential applications of the developed theory in design are discussed.

2 Material, Welding, Ultimate Strength Testing, and Results

A high strength steel with sheet thicknesses 1.2 mm, 1.5 mm and 2.0 mm was selected for the test. The engineering as well as the true stress-strain curve at quasi-static loading rate (0.025 mm/s) is shown in Fig. 1. The true stress-strain curve includes the Bridgman's correction for necking following the procedure outlined in [16,17]. Relevant material properties are obtained from the stress-strain curve as upper and lower yield strength of 359 MPa (52 ksi) and 345 MPa (50 ksi), respectively, ultimate tensile strength 434 MPa (63 ksi), reduction in area or ductility 61 percent, and the fracturing stress and strain as 676 MPa (98 ksi) and 0.95, respectively. The stress-strain curve indicates that the material is ductile with a median strain hardening, i.e., a strain-hardening exponent of 0.17. Its carbon content is less than 0.1 percent and magnesium less than 1 percent. The material is close to HSLA (high strength low alloy) Grade 50 steel or cold rolled 340 steel.

Cross tension samples composed of two 50.8 mm (2 inches) wide by 152.4 mm (6 inches) long coupons and lap-shear samples from two 38.1 mm (1.5 inches) by 152.4 mm (6 inches) coupons are spot-welded, as shown in Fig. 2, with a square overlap area. These sample dimensions follow the recommendation by SAE [18] and have sufficient widths to not affect the strength of the weld [19].

Welding was done using a 100 KVA spot welder machine using Z-Trode electrode cap that is Zirconium Copper based with a 7.87 mm radius hemispherical dome cap. The cap also has a flat tip face of 4.8 mm in diameter. Before welding, hand robbing using cloth with acetone was applied to remove grease and dirt from the coupon surface.

It is well known that both the interfacial failure and excessive expulsion reduce the strength of a spot weld, partly due to the small size of the nugget formed in welding and the porosity present in the weld, respectively. The welding schedules, listed in Table 1, are determined after several trials guided by industry standards such as AWS [18] and strength tests using lap-shear sample geometry such that neither interfacial failure nor excessive expulsion would occur. The resulted nominal (average) weld nugget diameters are 7.1 mm, 7.26 mm, and 7.58 mm, respectively for the 1.2 mm, 1.5 mm, and 2.0 mm sheets. These weld nugget sizes satisfy the conditions set by the predictive model [15] that ensures pullout failure mode of the weld nugget.

Strength testing was performed on a MTS universal tensile testing machine with a rate 1.524 mm/min (0.001 inch/sec) that is nearly quasi-static. Test fixtures for the cross tension samples were fabricated according to AWS [18]. The displacement in the lap-shear sample was recorded using an extensometer with 50.8 mm (2.0 inches) gage length. The stroke (or machine) displacement was used for the cross tension sample. The load and displacement histories were simultaneously recorded during the testing. Tests were terminated as the two coupons of a test sample separated completely.

Figure 3 shows schematically the load-displacement curves as observed from the tests. It is seen that in the lap-shear test the load-displacement curve exhibits a nonlinear region before reaching the peak load. This part is very similar to the stress-strain curve of ductile metals such as that shown in Fig. 1 and is attributed to the strain hardening of the material. The load starts to drop as the crack initiates. As the crack propagates along the circumference of the nugget (i.e., pullout failure) the load drops gradually. The shape of the ''tail'' of the curve depends upon the post failure mode, i.e., a long tail corresponds to a partial (typically one-half) nugget pullout and subsequent tearing of base metal along the loading direction and a short tail corresponds to complete nugget pullout. In the cross tension case, the displacement is large relative to the lap-shear sample and a nearly linear curve is maintained until failure. The load drops to zero quickly immediately after failure and the failure mode is typically clean and complete nugget pullout.

Batches A-C in Fig. 4 shows the test results in term of ultimate strength (or peak load), which corresponds to the crack initiation of the spot welds based on the observation during the tests. It is seen that the ultimate strength of the spot weld is a function of (*a*) sample geometry—lap-shear samples have higher strength than the cross tension samples, (*b*) thickness of the sheet—thicker coupon has higher strength, and (*c*) weld nugget size—weld with larger nugget fails at a higher load. These trends are well known and documented in industry. An unresolved and challenging issue in this type of data is ''can one develop a mechanics based model such that this behavior can be predicted quantitatively?'' In the following sections we attempt to address this issue by studying the failure mechanisms and then develop an analytical solution for predicting the ultimate strength of spot weld.

3 Failure Mechanisms

Lap-Shear Sample. Observation during tensile test of lap-shear samples reveals the failure process as schematically demonstrated in Fig. 5. As the sample is pulled initially, the weld nugget

Table 1 Welding schedule for the steel sheet

Thickness of the sheet (mm)	Weld Time (cycles) at 60 Hz	Hold Time (cycles) at 60 Hz	Weld Current (kA)	Weld Force (N)	Nominal Nugget Diameter (mm)	$\frac{1}{2}$ Nominal Nugget Thickness (mm)	% Nugget Indentation
1.2	14	2	10	2,982	7.1	0.94	22
1.5	21	5	11	4,228	7.26	1.17	22
2	28	5	12	5,340	7.58	1.3	35

experiences a rotation (see Fig. 5(*b*)), which essentially aligns the nugget with the loading line. In stage (*c*) the material surrounding the nugget is subjected to a predominantly tensile load and the deformation near the nugget is similar to a rigid button embedded in a ductile sheet. As the load increases, localized necking of the sheet metal occurs at the two apices, i.e., $\theta=0$ deg and 180 deg at locations near the juncture of the nugget and the base metal. Note that these two points are on the two different pieces of the coupons. Fracture then initiates at one of these two points (stage (*c*)) when the ductility of the sheet material is reached. Eventually pullout failure of the weld occurs as the initial crack grows around the circumference of the weld nugget.

Figure 6 is taken from the surface of a test sample. The loading was stopped and reduced to zero as the fracture was first observed during the tensile test of this sample. The dark hairline at the lower circumference of the nugget is the crack indicating the fracture initiation site. As can be seen from the figure, the fracture initiation site is at the location $\theta=0$ and some crack propagation (2 to 4 mm) along the circumference of the weld nugget already occurred on this sample.

Note that similar feature of those demonstrated in Fig. 5 is first reported by Zuniga and Sheppard [11] and later by Lin et al. [14].

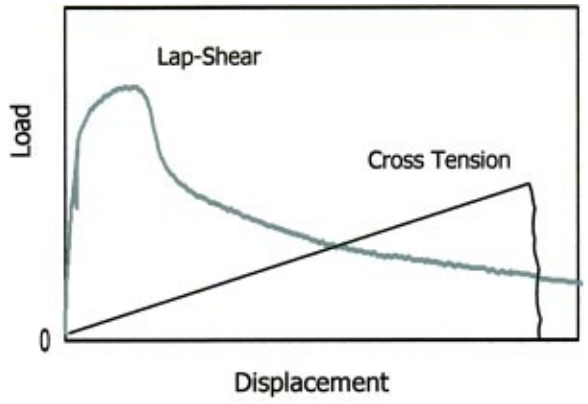

Fig. 3 Schematics showing the load-displacement curves of lap-shear and cross tension samples

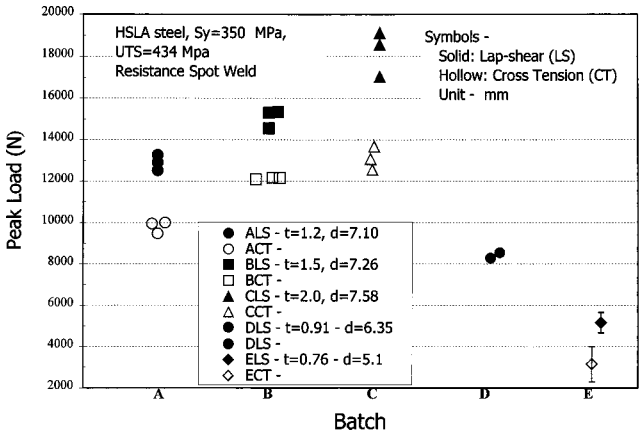

Fig. 4 Ultimate strength of the spot welds; batch A,B,C-USC data Batch D, Zuniga and Sheppard [11]; batch E, Sawhill and Furr [24] (some data are shifted horizontally for clarity)

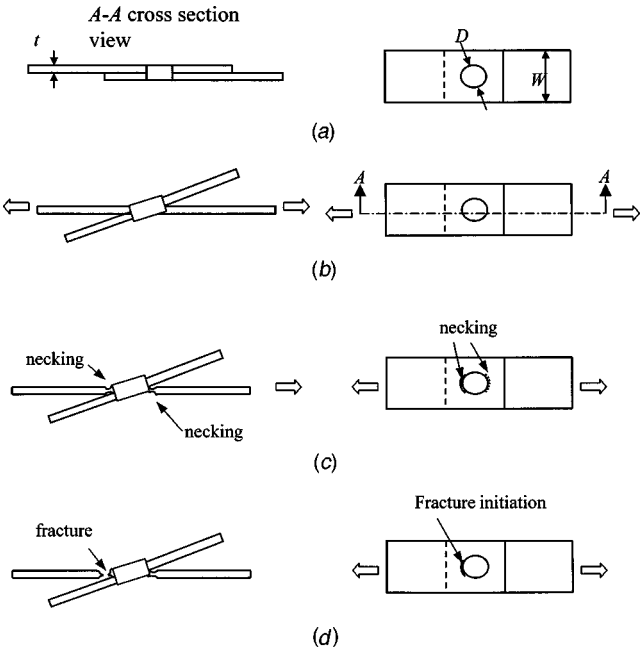

Fig. 5 Global deformation and failure process of a lap-shear spot-weld sample: (*a*) initial configuration, (*b*) nugget rotation (align first with the loading line); (*c*) stretching, thinning, and necking, and (*d*) tensile fracture due to localized necking.

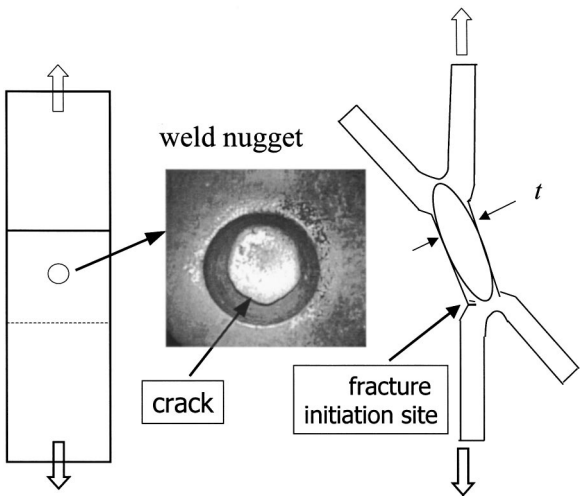

Fig. 6 Fracture initiation site of a lap-shear spot-weld sample. The hairline at the bottom of the nugget is the crack.

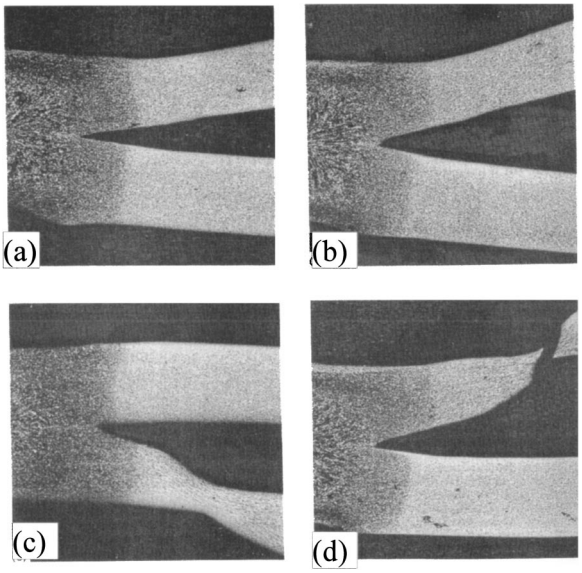

Fig. 7 Optical micrographs showing the stages of failure process of a lap-shear sample: (*a*), (*b*), and (*c*) show the progress of the localized necking and (*d*) final fracture (reproduced from Zuniga and Sheppard [11])

Optical micrographs from a sequence of deformation pattern of lap-shear sample from [11] are reproduced here as Fig. 7. Figure 7 clearly shows the stages of failure process development in a lap-shear sample—(*a*), (*b*), and (*c*) showing the progress of the localized necking at a position near the weld nugget edge and final fracture in (*d*).

The observation and Figs. 5–7 demonstrate that the failure mechanism of lap-shear sample at the material level is "*tensile*," even though the global loading mode to the test sample is *shear*. To further verify this point, a broken sample was cut, prepared and the fracture surface at $\theta = 0$ deg was examined under a scanning electronic microscope (SEM). Figure 8 shows a fractograph with 1,000×. The near circular dimples shown in Fig. 8 indicate a ductile and *tensile* fracture mechanism at the material level.

Cross-Tension Sample. The deformation pattern and failure process of a cross tension sample is demonstrated in Fig. 9. As the sample is loaded, large bending deformation of the sheet occurs initially (Fig. 9(*b*)). Eventually the weld nugget is pulled out from

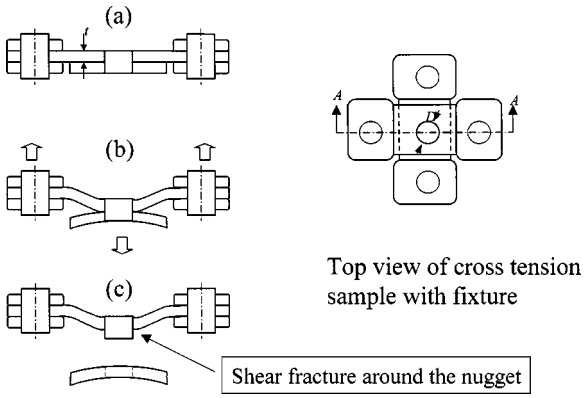

Fig. 9 Global deformation pattern (*b*) and the weld nugget pullout failure (*c*) of a cross tension sample

one coupon and stays with the other coupon (Fig. 9(*c*)). To demonstrate this, a micrograph of the cross section of a failed 1.5 mm specimen from Lin et al. [14] is reproduced here as Fig. 10. Besides the initial global bending of the sheet, the failure can be well characterized as through thickness shear around the weld nugget. To further verify this failure mechanism, SEM examination on the fractured surface produces the picture shown in Fig. 11. The elongated or "fish scale" dimples shown in Fig. 11 indicate that the fracture mechanism at the material level is ductile and *shear*, despite that the global loading mode to the sample is *tensile*.

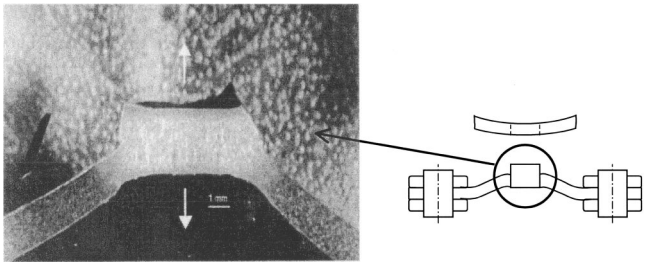

Fig. 10 Optical micrograph of the cross section of a failed 1.5 mm specimen showing the pullout failure of the weld nugget around the nugget circumference (reproduced from Lin, et al. [14])

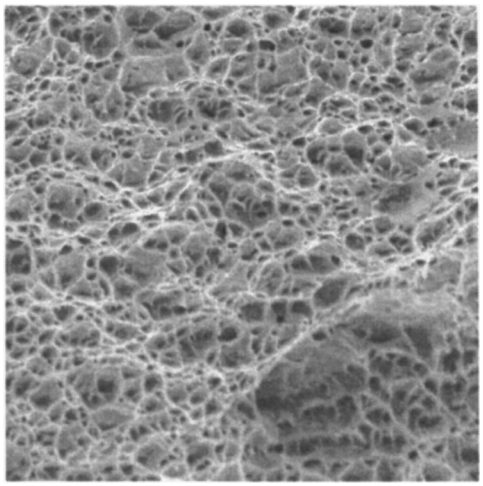

Fig. 8 SEM fractograph (1000X) of a lap-shear sample: the circular dimple rupture microstructure indicating tensile fracture

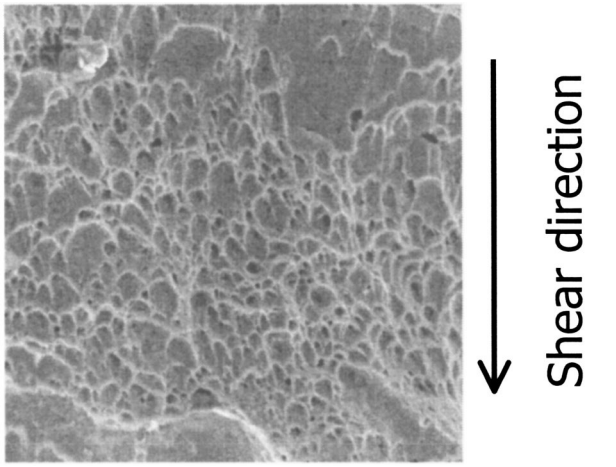

Fig. 11 SEM fractograph (1000X) of a cross tension sample: the "fish scale" rupture microstructure indicating shear fracture

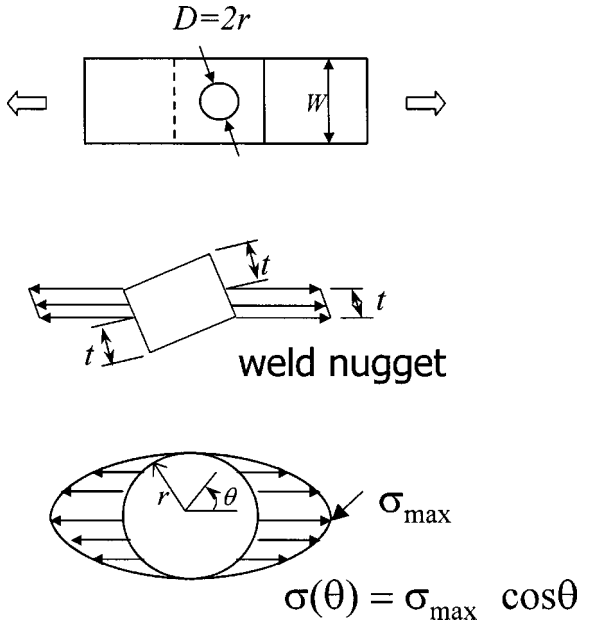

Fig. 12 Assumed stress distribution around the weld nugget in a lap-shear sample

4 Stress Analyses and Failure Load

Failure of spot weld is likely related to many parameters, e.g., residual stress, material inhomogeneity, welding parameters, thickness, nugget size, and material properties of the HAZ and the base metal. Attempts to include all these parameters in a failure criterion would require substantial analytical, numerical, and experimental efforts. Besides, any complex criterion would severely limit its use in engineering applications. As such, we chose to focus on developing an engineering approach by assuming a simplified stress distribution based on the identified failure mechanisms in lap-shear and cross tension samples. These stresses can then be related to the far field applied load and subsequently failure load or ultimate strength of the spot weld test sample.

For lap-shear samples, since the failure is predominantly by uni-axial tensile load and the weld nugget is circular, a harmonic tensile stress distribution around the weld nugget, as shown in Fig. 12, is assumed. The distribution of the stress can be written as

$$\sigma(\theta)=\sigma_{\max}\cos\theta \tag{1}$$

where $\theta=-90$ deg to 90 deg and $\sigma_{\max}$ is the maximum tensile stress occurring at $\theta=0$ deg. Due to symmetry there is another similar stress distribution in $\theta=90$ deg to 270 deg with $\sigma_{\max}$ at $\theta=180$ deg acting on the other piece of the coupon. Equilibrium condition requires that

$$P=\int_{-\pi/2}^{\pi/2}\sigma(\theta)\cdot\frac{d}{2}t\cdot\cos\theta\cdot d\theta=\frac{\pi}{4}td\sigma_{\max}=0.785td\sigma_{\max} \tag{2}$$

where P is the applied tensile load at far field. Equation (2) relates the local maximum stress to the far field load. At the initiation of fracture, Eq. (2) becomes

$$P_f=0.785td\sigma_f \tag{3}$$

where t is the thickness of the base metal sheet or one half thickness of the weld nugget, d the diameter of the weld nugget, P_f the failure load or strength of the sample and σ_f the fracturing stress of the material in tension. Here, ''failure'' of the test sample is defined as the ''fracture initiation'' which corresponds to the peak load as discussed earlier.

For cross tension test samples, since the failure is predominantly by shear around the circular weld nugget, a harmonic shear stress distribution around the weld nugget is assumed. As shown in Fig. 13, the shear stress distribution has four identical sectors to reflect the symmetric condition of the loading. The distribution of the stress in one sector can be written as

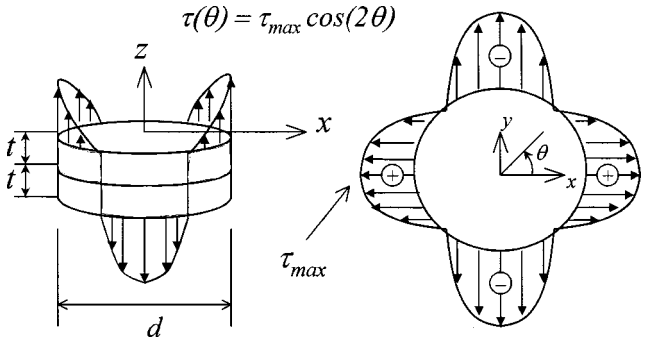

Fig. 13 Assumed stress distribution around the weld nugget in a cross tension sample

$$\tau(\theta)=\tau_{\max}\cdot\cos 2\theta \tag{4}$$

where $\tau_{\max}$ is the maximum shear stress occurring at $\theta=0$ deg, 180 deg (and $\theta=90$ deg, 270 deg on the other piece of the coupon). Equilibrium condition requires that

$$P=2\int_{-\pi/4}^{\pi/4}\tau(\theta)\cdot rtd\theta=td\tau_{\max} \tag{5}$$

where P is the applied tensile load in far field. At the initiation of fracture, Eq. (5) becomes

$$P_f=td\tau \tag{6}$$

where τ_f is the fracturing stress of the material in shear.

Examining the failure loads of (3) and (6), it appears that the failure load is proportional to the thickness of the sheet metal and the weld nugget diameter. Furthermore, two material properties, fracturing stress in tension σ_f and fracturing stress in shear τ_f, are present in Eqs. (3) and (6), respectively. These two can be related to each other by using classical failure criteria. For example, for ductile materials von Mises failure criterion requires $\tau_f=0.577\sigma_f$ and Tresca requires $\tau_f=0.5\sigma_f$ [16]. Using these failure criteria and (3) and (6), one has

$$\begin{aligned}P_f^{\text{cross tension}}&=0.735\ P_f^{\text{lap-shear}}\quad\text{von Mises}\\&=0.64\ P_f^{\text{lap-shear}}\quad\text{Tresca}\end{aligned} \tag{7}$$

Equation (7) relates the failure load or the ultimate strength of a spot weld tested in cross tension to lap-shear sample geometry.

5 Effect of Weld Indentation

For steel, the thickness of the nugget of a spot weld is often less than the thickness of the base metal sheet due to the applied pressure by the electrodes during the welding. The effect of this weld indentation is more pronounced in thick-gauged sheet than in thin-gauged sheet depending on the welding parameters. As shown in Table 1, the percentage of reduction in thickness from the base metal to the nugget is about 22 percent, 22 percent, and 35 percent corresponding to the thickness 1.2 mm, 1.5 mm, and 2 mm, respectively.

For thin gauged sheet, i.e., around 1 mm or less, the change in thickness due to electrode indentation is typically not significant. As can be seen in Fig. 7, the thickness of the nugget is nearly twice of the base metal sheet thickness (0.91 mm), i.e., no indentation, and the failure site is actually in the base metal. On the other hand the fracture initiation site in a thicker sheet (2 mm), as shown in Fig. 6, is clearly at the corner where the change of

Table 2 Maximum tensile stress (N/mm^2) predicted by Eq. (2) and finite element analysis [5] (*P*: load, *d*: nugget diameter, *t*: sheet thickness, *b*: length, *W*: width)

Eq. (2)	FEA	P (N)	d (mm)	t (mm)	b (mm)	W (mm)
14.7	14.5	100	5.4	1.6	79.6	31
9.9	9.5	100	8.0	1.6	79.6	31
14.7	13.8	100	5.4	1.6	49.6	31
9.9	8.5	100	8.0	1.6	49.6	31

thickness takes place. Stress concentration associated from the geometry change at the location could also contribute to the initiation of fracture.

Strictly speaking, in applying the formulas (3) and (6), t is the thickness where the necking or fracture occurs, i.e., use t if fracture is in the base metal and t_n (thickness of the nugget) if fracture is along the circumference of the nugget. It was observed that the fracture site depends on the welding schedule and thickness. However, since in practice the nugget thickness t_n is not measured and reported, the base metal thickness t becomes the nature candidate in all formulas in the current paper. Note that the recommended practice by American Welding Society is the depth of depression on sheet surfaces caused by welding electrodes not to exceed 25 percent of the sheet metal thickness [21]. The thickness of both the base metal sheet and the weld nugget from our test is provided in Table 1. The weld in the 2 mm thick sheet has excessive indentation apparently. It is anticipated that the error involved in using the base metal thickness in Eqs. (3) and (6) would not be significant, relative to other factors, if the recommended practice in [21] is followed.

6 Comparison With Numerical and Other Results

Zhang [5] performed detailed finite element analyses for spot weld subjected to mixed far field normal/shear load. As $\theta=0$ in [5], the problem reduces to the lap-shear sample and loading condition discussed in Section 4. The maximum tensile stress, calculated numerically, which occurs at $\theta=0$ shown in Fig. 12, is reported in [5] for four cases that have different sample dimensions and weld nugget diameters. Table 2 lists the results calculated using Eq. (2) and the numerical solutions for the four cases from [5]. The comparison indicates that Eq. (2) is indeed a very good approximation.

Close examination of Eq. (2), one can find that this equation, derived from the simple stress distribution shown in Fig. 12, is precisely the analytical solution developed from a more rigorous analysis by Radaj and Zhang [22,23]. In [22,23] stress distribution around a weld nugget is derived by assuming the weld nugget as a circular rigid button embedded in an infinitely large plate and subjected to far field tension. Since for steels, the yield stress in the nugget is generally one to three times of the base metal, the ''rigid button'' assumption is indeed a good assumption for stress analysis. This is also evidenced by the failure process discussed in Section 3.

7 Comparison With Test Data from Cross Tension and Lap-Shear Samples

Assuming σ_f is a constant for a given material, using Eqs. (3), (6), and (7) one has

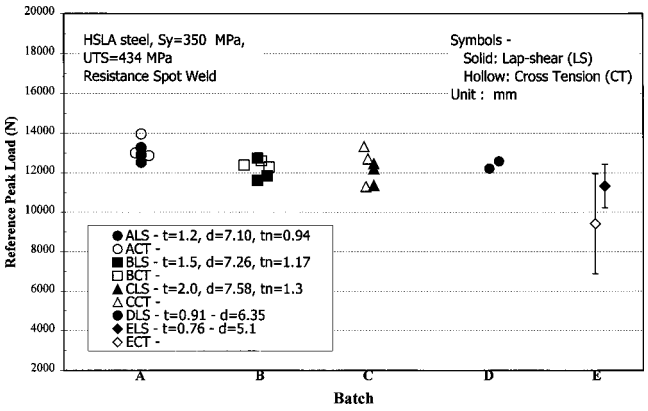

Fig. 14 Failure loads normalized with respect to batch A, lap-shear sample (ALS)

$$\left(\frac{P_f}{td}\right)_{\text{reference}} = \frac{P_f}{td} \quad \text{for lap-shear sample}$$

$$= \left(\frac{0.785\ P_f}{0.577}\right)$$

$$= 1.36\frac{P_f}{td} \quad \text{for cross tension sample (von Mises)} \tag{8}$$

Equation (8) can be used to convert the test data from one test condition, i.e., t, d, and P_f, to a reference condition of a lap-shear sample, i.e., another t, d, and P_f of a lap-shear sample. Test data of batches A-C shown in Fig. 4 are normalized using (8) with respect to batch A, lap-shear sample (ALS) and plotted in Fig. 14 with the same scale. As can be seen in Fig. 14 the scatter of data after normalization is greatly reduced compared to that shown in Fig. 4. It indicates that the developed model, i.e., Eqs. (3), (6), and (7), is indeed respectable. In Fig. 14, t_n (half of the nugget thickness) is used for batches A-C for a more precise comparison since we have each nugget thickness measured individually. Batch C data would be slightly lowered in Fig. 14 if the sheet thickness t were used because of its deeper indentation. However, it would not affect the overall conclusion.

Zuniga and Sheppard [11] performed tests to study the failure mechanisms of spot weld in lap-shear and coach peel geometry. They used a steel that is very close to ours and hence a direct comparison is possible. Two groups of ultimate tensile strength, 8282 ± 147 N and 8536 ± 62 N, with a slightly different welding schedules for the spot weld ($t=0.91$ mm, $d=6.35$ mm) are reported for the lap-shear sample. These two are included in Fig. 4 as batch D. The ultimate strength of batch D is considerably low relative to batches A-C because of its relatively thin gage and small nugget size. However, when converting (or normalizing) to the reference weld nugget and sheet gage of batch ALS using Eq. (8), the ''predicted'' ultimate strength for the reference weld batch ALS is in-line with other test data as shown in Fig. 14.

Sawhill and Furr [24] tested spot weld samples to study the weldability of steel sheets. The materials tested include a wide range of yield strength, i.e., from plain carbon steel to HSLA and the test sample geometries include cross tension, lap-shear, coach-peel as well as in-plane torsion. Envelope encompassing the weld strength of cold-rolled steels using lap-shear and cross tension samples is shown in Fig. 15. The predicted failure load envelop for cross tension samples, using the lap-shear data in Fig. 15 and Eq. (7), is also plotted in Fig. 15 for comparison. As can be seen, the prediction is very reasonable with Tresca being slightly better than von Mises theory.

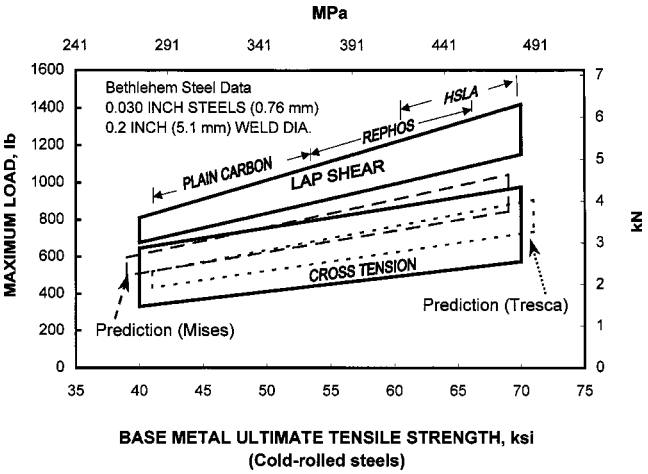

Fig. 15 Failure strength of lap-shear and cross tension samples made of cold rolled steels with various ultimate tensile strength [24] and prediction by (7) (The predicted is shifted to the left (Mises) and right (Tresca) for clarity)

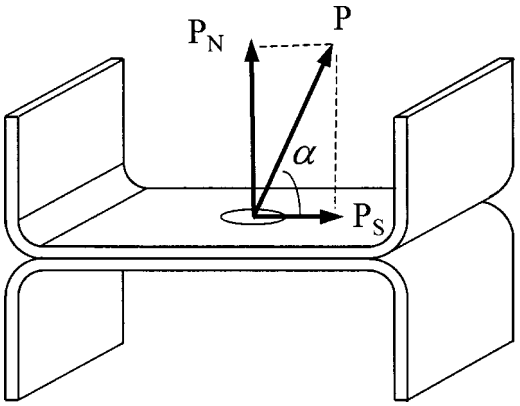

Fig. 16 Tensile/shear mixed mode test sample geometry [13]

8 Mixed Normal/Shear Loading

Having the stress distributions developed for spot weld subjected to normal force, i.e., cross tension sample, and shear force, i.e., lap-shear sample, an extension to mixed normal/shear loading conditions is investigated in this section. The analytical result is then compared with test data.

For spot weld loaded with a combination of normal and shear forces, superposition of Eqs. (1) and (4) can be used for the stress, which leads to a biaxial stress field. Using von Mises and Tresca failure criteria for a biaxial stress field, one has

$$\frac{1}{3}[2\sigma^2+6\tau]^{1/2}=\frac{\sqrt{2}}{3}\sigma_f \quad \text{von Mises}$$

$$\left(\frac{\sigma}{2}\right)^2+\tau^2=\left(\frac{\sigma_f}{2}\right)^2 \quad \text{Tresca} \tag{9}$$

Substituting Eqs. (1) and (4) into (9) and acknowledging that points at $\theta=0$, 180 deg are the most critical points around the weld nugget for failure, one obtains

$$1.623\left(\frac{P_S}{td}\right)^2+3\left(\frac{P_N}{td}\right)^2=\sigma_f^2 \quad \text{von Mises}$$

$$1.623\left(\frac{P_S}{td}\right)^2+4\left(\frac{P_N}{td}\right)^2=\sigma_f^2 \quad \text{Tresca} \tag{10}$$

where $P_S=P\cos\alpha$ is the shear component and $P_N=P\sin\alpha$ the normal component of the applied force P as shown in Fig. 16.

Mixed mode test data from Lee et al. [13] is used here to validate the developed model. Mild steel with yield stress 170 MPa, ultimate tensile strength 282 MPa and 0.89 mm thick sheet was tested using two weld nugget sizes, 4.3 mm and 6.4 mm. Failure loads are reproduced in Fig. 17. The average of the test data in the pure shear case is used in (3) to obtain the fracturing stress σ_f, 1562 MPa. Using this fracturing stress, the prediction of the failure envelope or Eq. (10) is then plotted in Fig. 17. As shown in the figure, test data in the mixed mode region are somewhat lower than the predicted. Nevertheless, considering the simplicity of the proposed model, the comparison is reasonably good.

Note three different widths of test coupons are used in [13], i.e., 19 mm (0.75 inch), 31 mm (1.22 inch), and 43 mm (1.69 inch). Failure loads, shown in Fig. 17, show an increasing trend with increasing width. As studied by Zhou et al. [19] failure strength of a spot weld is not affected by the width of a test sample when the width is beyond a critical value. The strength decreases with the width, as it is less than the critical value. For the sheet thickness and nugget size used by Lee et al. [13], the first two widths are apparently less than the critical width to ensure a ''width independent'' failure load. Our analytical model does not include the effect of the width and this could contribute to the fact that better comparison is obtained for wider samples shown in Fig. 17. In fact, if the prediction were made to each group of data with equal width individually a better comparison would be obtained.

9 Discussion

The most intriguing result from the current work is that while spot weld in a lap-shear test sample is subjected to a global shear load the failure mechanism of the weld at the microstructure level is in fact tensile. On the other hand, while the spot weld in a cross tension sample is subjected to *normal* load the failure mechanism of the weld is shear. These failure mechanisms help us to develop the applied load-stress relations, Eqs. (1–7). And, accordingly the failure load relations are able to explain why cross tension sample always fails at a lower load than the lap-shear sample containing similar spot weld which is well known in industry but had lacked mechanics based explanations.

As stated previously, the strength of spot welds can be related to many factors such as residual stress, welding parameters and material inhomogeneity. A rigorous mechanics based model, which includes all these factors in predicting spot weld failure would require significant development and complex material constitutive models for the inhomogeneous materials in the weld, thermal-electrical-mechanical models for the welding and advanced fracture criterion including the residual stress. Using the

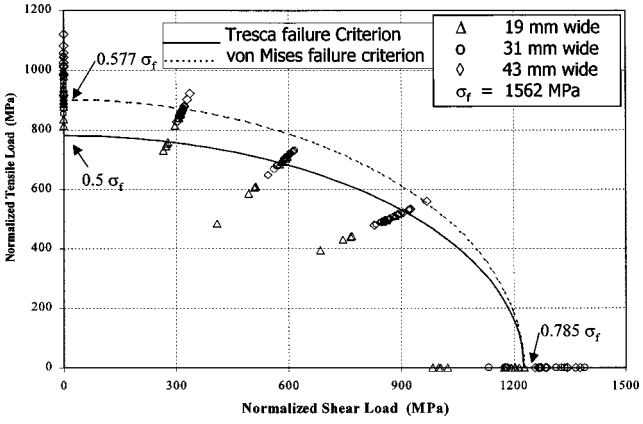

Fig. 17 Tensile/shear mixed mode test data [13] and prediction by (10) Normalized load=failure load/(nugget diameter *x* sheet thickness)

model in the current paper, however, detailed studies on the effect of these factors to the failure load are circumvented. This convenience is achieved mainly by using a fracturing stress σ_f. Although the property σ_f is most likely dependent upon the welding parameters and base metal material, in practice it can be obtained easily from a simple lap-shear tensile test and using Eq. (3) for a batch of welds fabricated from a designated set of welding parameters and sheet material.

Note that the ''fracturing stress'' for the HSLA material studied is 676 MPa from the uniaxial tensile tests shown in Fig. 1. The ''fracturing stress'' as defined in Eq. (3) is about 1780 MPa from the spot weld test data shown in Figs. 4 and 14. Theoretically, some relationships between these two ''material properties'' should exist. Recall that in the early development of fracture mechanics, i.e., in the 1960's, a critical stress criterion was often used in predicting fracture event of solids. However, as of today, it is still unclear why the critical stress determined from fracture tests is much higher than the fracture stress from uniaxial tensile test on smooth specimens. Further studies along this direction to link the basic material test data from smooth specimens to failure of cracked solid or spot weld are definitely valuable.

An essential element in the current study, which distinguishes itself from others, is to interpret the failure of spot weld at the *stress* level. Using the tensile fracturing stress, the shear fracturing stress and the classical failure theory we are able to link the failure strength of spot weld from lap shear geometry to that from cross tension geometry as well as the combined shear/normal loading conditions. Practically, it implies that once the fracturing stress σ_f is determined from a simple lap-shear test, ultimate strength of the spot weld (*a*) in cross tension sample, (*b*) with different nugget size and base metal sheet thickness, and (*c*) under mixed normal/shear load, can be *predicted* using Eqs. (7), (8), and (10), respectively. This conclusion presents tremendous potential savings for automotive industry that requires strength data of spot weld of different sizes in different sheet gages in safety design. For example, using the test data shown in Fig. 15, a steel with UTS $=434$ MPa has the failure strength of $5{,}135\pm498$ N if it is lap-shear and 3150 ± 850 N if it is cross tension sample. These failure loads are based on sheet thickness $t=0.76$ and weld nugget diameter $d=5.1$ mm and are plotted in Fig. 4 as batch E. The predicted failure loads, after converting to $t=1.2$ mm and $d=7.1$ mm and lap shear sample, i.e., batch ALS, are then $11{,}326\pm1094$ N and 9417 ± 2541 N. As shown in Fig. 14, these predicted loads compare favorably to the test data of batches A-D, although they are about 10 percent to 15 percent lower than anticipated. It may be concluded that the comprehensive test data provided in Fig. 15 in conjunction with Eq. (8) can be used by industry for preliminary safety design of auto assemblies.

In the finite element (FE) simulation of auto body under a crash scenario, there are many unresolved issues. For examples, ''what is the appropriate (or least complex) FE model for the weld?'' and ''what is the failure criterion?'' Using the equations developed in this paper, a simple beam element may be used to simulate a weld nugget connecting two sheets and failure of the weld can then be quantified provided that the fracture stress σ_f is determined by lap-shear tests in advance.

This paper addresses the tension and shear in cross tension and lap-shear spot weld test sample geometries. Spot weld in auto body assembly is generally subject to a combination of tension, shear, torsion, as well as bending. To have a truly useful and general engineering model for industry, further development for spot weld under torsion and bending at the coupon level, e.g., coach peel sample, and validating the model through comparison with test data from coupons and structural components, in quasi-static, fatigue and impact loading conditions are necessary.

Acknowledgment

Partial support of this work by NSF through grant CMS0116238 and the encouragement from the Program Director, Dr. Kenneth P. Chong are greatly appreciated. Nippert Company generously supplied welding cap electrodes. Dr. Kenneth W. Miller, formerly at USC, of St. Cloud State University, performed the welding and some of the tests shown in Fig. 4. Dr. X. Zhu contributed to many discussions. Dr. P.C. Wang of General Motor Corporation provided invaluable insight of spot welding from industry point of view.

References

[1] Ewing, K. W., Cheresh, M., Thompson, R., and Kukuchek, P., 1982, ''Static and Impact Strengths of Spot-Welded HSLA and Low Carbon Steel Joints,'' SAE Paper 820281.
[2] VandenBossche, D. J., 1977, ''Ultimate Strength and Failure Mode of Spot Welds in High Strength Steels,'' SAE paper 770214.
[3] Radaj, D., 1989, ''Stress Singularity, Notch Stress and Structural Stress at Spot-Welded Joints,'' Eng. Fract. Mech., **34**(2), pp. 495–506.
[4] Radaj, D., and Zhang, S., 1993, ''On the Relations Between Notch Stress and Crack Stress Intensity in Plane Shear and Mixed Mode Loading,'' Eng. Fract. Mech., **44**(5), pp. 691–704.
[5] Zhang, S., 2001, ''Approximate Stress Formulas for a Multiaxial Spot Weld Specimen,'' Weld. J. (Miami), **80**(8) 201s–203s.
[6] Zhang, S., 1999, ''Approximate Stress Intensity Factors and Notch Stresses for Common Spot-Welded Specimens,'' Weld. J. (Miami), **78**(5), pp. 1735–1795.
[7] Zhang, S., 1999, ''Stress Intensities Derived from Stresses Around a Spot Weld,'' Int. J. Fract., **99**, pp. 239–257.
[8] Zhang, S., 1997, ''Stress Intensities at Spot Welds,'' Int. J. Fract., **88**, pp. 167–185.
[9] Wung, P., 2001, ''A Force-Based Failure Criterion for Spot Weld Design,'' Exp. Mech., **41**(4), pp. 107–113.
[10] Wung, P., Walsh, T., Ourchane, A., Stewart, W., and Jie, M., 2001, ''Failure of Spot Welds Under In-Plane Static Loading,'' Exp. Mech., **41**(1), pp. 100–106.
[11] Zuniga, S., and Sheppard, S. D., 1997, ''Resistance Spot Weld Failure Loads and Modes in Overload Conditions,'' Fatigue and Fracture Mechanics: 27th Volume, ASTM STP 1296, R. S. Piascik, J. C. Newman, and N. E. Dowling, eds., American Society for Testing and Materials, pp. 469–489.
[12] Barkey, M. E., and Kang, H., 1999, ''Testing of Spot Welded Coupons in Combined Tension and Shear,'' Exp. Tech., **23**(5), pp. 20–22.
[13] Lee, Y., Wehner, T., Lu, M., Morrissett, T., Pakalnins, E., 1998, ''Ultimate Strength of Resistance Spot Welds Subjected to Combined Tension and Shear,'' J. Test. Eval., **26**(3), pp. 213–219.
[14] Lin, S. H., Pan, J., Wu, S., Tyan, T., and Wung, P., 2002, ''Failure Loads of Spot Welds under Combined Opening and Shear Static Loading Conditions,'' Int. J. Solids Struct., **39**, pp. 19–39.
[15] Chao, Y. J., 2002, ''Failure of Spot Weld: A Competition Between Crack Mechanics and Plastic Collapse,'' *Recent Advances in Experimental Mechanics—In Honor of Isaac M. Daniel*, Kluwer Academic Publishers, pp. 245–256.
[16] Dowling, N. E., *Mechanical Behavior of Materials*, Prentice Hall, New Jersey.
[17] Zhang, Z. L., Hauge, M., Degard, J., and Thaulow, C., 1999, ''Determining Material True Stress-Strain Curve from Tensile Specimens With Rectangular Cross-Section,'' Int. J. Solids Struct., **36**, pp. 3497–3516.
[18] ANSI/AWS/SAE/D8.9-97, 1997, Recommended Practices for Test Methods for Evaluating the Resistance Spot Welding Behavior of Automotive Sheet Steel Materials, American Welding Society, Miami.
[19] Zhou, M., Hu, S. J., and Zhang, H., 1999, ''Critical Specimen Sizes for Tensile-Shear Testing of Steel Sheets,'' Weld. J. (Miami), **78**(9), pp. 305s–312s.
[20] *Materials and Applications*, 1998, Part II, Welding Handbook, **4**, 8th edition, American Welding Society.
[21] AWS D8.7-88, SAE J-1188, 1987, Recommended Practices for Automotive Weld Quality—Resistance Spot Welding, American Welding Society.
[22] Radaj, D., and Zhang, S., 1996, ''Anschauliche Grundlagen fur Krafte und Spannungen in Punktgeschweisten Uberlappverbindungen, Konstruktion,'' **48**, pp. 65–71.
[23] Radaj, D., and Zhang, S., 1996, ''Strukturspannungen am starren Kern in endlich berandeter Platte,'' Konstruktion, **48**, pp. 195–199.
[24] Sawhill, J. M., Jr., and Furr, S. T., ''Spot Weldability Tests for High-Strength Steels,'' SAE paper 810352.